Tailoring of Biomimetic High-Density Lipoprotein Nanostructures Changes Cholesterol Binding and Efflux

Andrea J. Luthi,[†] Heng Zhang,[‡] Dongwoo Kim,[†] David A. Giljohann,[†] Chad A. Mirkin,[†,§] and C. Shad Thaxton[‡,§,⊥,*]

[†]Department of Chemistry, Northwestern University, 2145 Sheridan Road, Evanston, Illinois 60208, United States, [‡]Department of Urology, Feinberg School of Medicine, 303 East Chicago Avenue, Tarry 16-703, Chicago, Illinois 60611, United States, [§]International Institute for Nanotechnology, Northwestern University, 2145 Sheridan Road, Evanston, Illinois 60208, United States, and [⊥]Institute for BioNanotechnology and Medicine, Northwestern University, 303 East Superior, Suite 11-131, Chicago, Illinois 60611, United States

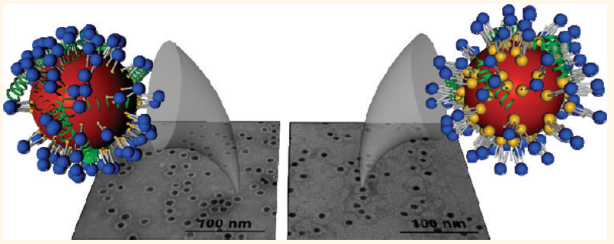

ABSTRACT Gold nanoparticles (Au NPs) were employed as templates to synthesize spherical, high-density lipoprotein (HDL) biomimics (HDL Au NPs) of different sizes and surface chemistries. The effect of size and surface chemistry on the cholesterol binding properties and the ability of the HDL Au NPs to efflux cholesterol from macrophage cells were measured. Results demonstrate that Au NPs may be utilized as templates to generate nanostructures with different physical characteristics that mimic natural HDL. Furthermore, the properties of the HDL Au NPs may be tailored to modulate the ability to bind cholesterol in solution and efflux cholesterol from macrophages. From the conjugates tested, the optimum size and surface chemistry for preparing functional Au NP-templated HDL biomimics were identified.

KEYWORDS: gold · nanoparticle · high-density lipoprotein · cholesterol efflux · biomimic · atherosclerosis

Coronary heart disease (CHD) is the leading cause of death worldwide and is caused in large part by atherosclerosis.[1−3] Atherosclerosis results from excess cholesterol circulating in the bloodstream.[2,4] At the cellular level, macrophages situated within the intimal layers of the arteries consume cholesterol and form foam cells, which initiate and drive the formation of atherosclerotic plaques.[2,4] Continued cholesterol accumulation, among other factors, eventually decreases plaque stability, and the rupture of unstable atherosclerotic plaque causes myocardial infarction or stroke.[2,4]

Cholesterol is transported by naturally occurring nanoparticles known as lipoproteins.[3,4] Specifically, low-density lipoproteins (LDL) are the main carriers of cholesterol in the human body.[3] High circulating levels of cholesterol-rich LDLs promote atherosclerosis and CHD.[2,4,5] Lowering LDLs is the most common therapeutic strategy for CHD, but it has not been able to adequately relieve the disease burden.[4,6] Conversely, high-density lipoproteins (HDL) show an inverse correlation with incidence of CHD.[3,7] Thus, raising HDL represents a potential therapeutic strategy. One mechanism by which HDL protects against atherosclerosis is thought to be reverse cholesterol transport (RCT), the process by which HDLs take up cholesterol from macrophages for transport to the liver for biliary excretion.[8,9]

Direct administration of reconstituted HDL (rHDL) represents a promising therapeutic strategy for CHD.[8,10,11] Reconstituted HDLs mimic the size and discoidal shape of immature nascent HDL, and their syntheses are well-established.[8,12] However, the synthesis of mature spherical HDL species is more difficult. Spherical structures can be synthesized by incubating rHDL with LDL and the enzyme lecithin cholesterol acyl transferase.[12,13] However, biosynthetic strategies for producing spherical mimics of HDL are limited with regard to scalability and the ability to rationally manipulate HDL surface chemistry. As such, spherical HDL structure, structure−function relationships, and therapeutic potential have been less studied than rHDL.[14−17]

The heterogeneity of natural HDL species with regard to form, composition, and function provide compelling reasons to develop synthetic routes to mature spherical HDL. Spherical HDL constitutes the majority of HDL in circulation,[17] and studies have shown

* Address correspondence to cthaxton003@md.northwestern.edu.

Received for review September 14, 2011 and accepted November 25, 2011.

Published online November 25, 2011
10.1021/nn2035457

that the level of large spherical HDL species specifically inversely correlates with the incidence of CHD.[18] Patients with CHD have lower levels of α-1 and α-2 HDL, the larger, spherical species, and higher levels of α-3 and pre-β-1 HDL, the smaller species.[19,20] Furthermore, HDL is believed to have other atheroprotective properties beyond RCT such as being anti-inflammatory and antioxidative.[18,21] There is evidence that these properties vary for different species of HDL; however, little is known regarding how the properties of different HDL species contribute to the development and progression of atherosclerosis.[18] Finally, a bottom-up synthetic route to spherical HDL provides an opportunity to control cholesterol content, in effect, rendering the biomimetic HDL cholesterol-poor and disposing it to maximal cholesterol sequestration. Thus, the tailored synthesis of monodisperse, spherical HDL allows the investigation of cholesterol transport mechanisms utilized by spherical HDL species and provides a tool to study the structural characteristics of HDL that optimize atheroprotection.

Chemistry provides the opportunity to control the assembly of scalable and tunable bioinorganic nanostructures. Inorganic nanoparticles can be modified with a variety of biological and organic ligands[22] including nucleic acids,[23−29] proteins,[30−32] peptides,[33,34] and polymers.[35,36] Previously, we demonstrated the use of a gold nanoparticle to synthesize an HDL biomimic (HDL Au NP).[37] Initial work showed that HDL Au NPs sequester a fluorophore-labeled cholesterol analogue (25-[*N*-[(7-nitro-2-1,3-benzoxadiazol-4-yl)methyl]amino]-27-norcholesterol (NBD cholesterol), K_d = 3.8 nM) and were similar to natural spherical HDL species in size, shape, and surface composition, pointing to the therapeutic potential of such structures.[37] Other groups have utilized nanoparticle scaffolds, including gold nanoparticles, to synthesize spherical HDL biomimics for imaging atherosclerotic plaque.[38−41] In addition, our group recently demonstrated the use of HDL Au NPs for nucleic acid delivery.[42] In this work, we investigate the effect of core size and surface composition on HDL Au NP function and show that these parameters may be altered to manipulate cholesterol efflux to HDL Au NPs. From these studies, we identify an optimal Au NP size and surface composition for synthesizing biomimetic HDL.

RESULTS

Synthesis and Characterization of the HDL Au NPs. HDL Au NP constructs were synthesized with different core sizes and surface modifications. As natural HDL varies in size from 7 to 13 nm in diameter,[3,43] we purchased 5 and 10 nm diameter colloidal gold nanoparticles (Au NP) as templates to synthesize the HDL biomimics. Though 5 and 10 nm diameter Au NPs were purchased, size analysis by TEM showed that the diameters were

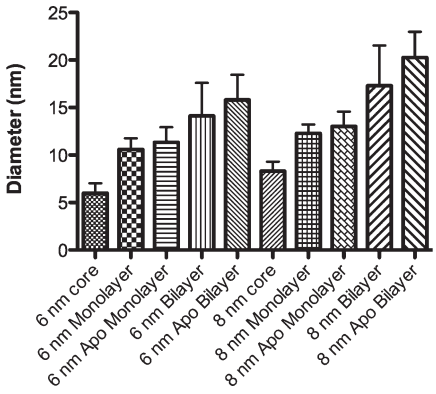

Figure 1. Diameters of HDL Au NPs measured by TEM.

actually 6 ± 1 and 8 ± 1 nm, respectively (Figure 1). The main surface components of natural HDL, apolipoprotein AI (Apo AI) and phospholipids, specifically phosphatidylcholines, were added to the surface of the Au NP templates. To assess the functional consequences of Apo AI, constructs were also synthesized without Apo AI. A sulfhydryl modification to Apo AI (Apo AI-SH) was utilized to conjugate Apo AI to the surface of the Au NPs, as thiols have a strong affinity for Au.[22,44] Three different phospholipids were used to generate different surface compositions on the HDL Au NPs (Scheme 1). First, an HDL biomimic was synthesized with 1,2-bis(16-mercaptohexadecanoyl)-*sn*-glycero-3-phosphocholine (L16SH) to generate a phospholipid monolayer on the Au surface. This lipid has a structure similar to the common natural phospholipid, 1,2-dipalmitoyl-*sn*-glycero-3-phosphocholine (DPPC), but with sulfhydryl groups in place of the methyl groups at the ends of the fatty acid tails. This enables direct attachment to the Au NP through the tails. The second HDL biomimic utilizes two phospholipids, 1,2-dipalmitoyl-*sn*-glycero-3-phosphoethanolamine-*N*-[3-(2-phyridyldithio)propionate] (PDP PE) and DPPC. The disulfide functional group of PDP PE provides a means of conjugation to the Au NP surface, while DPPC generates a capping layer to create a water-soluble construct. In total, different combinations of the phospholipids and Apo AI yield eight unique Au NP constructs (Scheme 1).

HDL Au NPs were characterized in terms of stability, diameter, and Apo AI composition. Monitoring the surface plasmon band (SPB) of the Au NP provides an indication of the stability of the Au NP after surface modification. Disperse gold nanoparticles exhibit a characteristic SPB in the ultraviolet−visible (UV−vis) spectrum around 520 nm and appear red in color.[22,24] On the other hand, aggregated gold nanoparticles appear purple and exhibit a red-shifted SPB.[22] Each solution of HDL Au NPs synthesized for this study was indefinitely stable in solution as demonstrated by their red color and a measured SPB of ~520 nm (Supporting Information Figures S1 and S2).

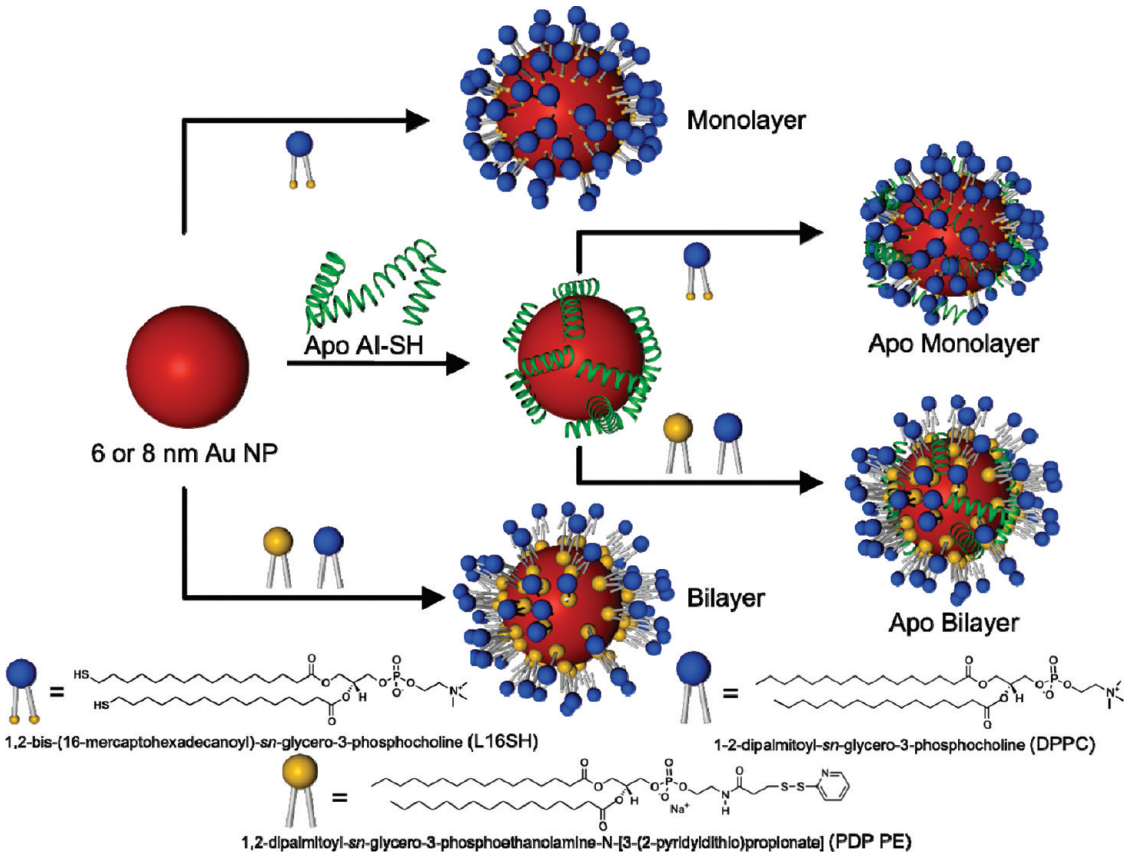

Scheme 1. Schematic for the synthesis of HDL Au NPs.

Transmission electron microscopy (TEM) was employed to determine the size and surface functionalization of the HDL Au NPs. Solutions of HDL Au NPs and Au colloids were dried on carbon-coated copper grids and stained with uranyl acetate. Uranyl acetate is a negative stain, and the phospholipids are visible as white rings around the Au NPs (Figure 2 and Supporting Information Figure S3).[45,46]

In general, an increase in the diameter was observed after addition of Apo AI-SH and the phospholipids, a reflection of surface functionalization (Figure 1). For both 6 and 8 nm cores, different phospholipid attachment chemistries resulted in HDL Au NPs of different sizes. In the case of both PDP-PE and DPPC addition to form a phospholipid bilayer, the HDL Au NPs assume a larger diameter than the monolayer HDL Au NPs. The staining clearly demonstrates this difference in lipid layer thickness. When a monolayer is added to the Au NP, the diameter increases by 4−5 nm, and when a bilayer is formed, the diameter increases by 8−12 nm. The shell of natural lipoproteins is a lipid monolayer reported to be 2 nm thick, which substantiates the 4−5 nm increase when a monolayer is added to the Au NP.[47] Structural data obtained for discoidal rHDL suggest that rHDL is a phospholipid bilayer disk with Apo AI wrapped around the disk in a belt-like fashion.[15] The rHDL disks are 4−5 nm wide, which supports the bilayer arrangement of phospholipids on the HDL Au NP and the resulting overall size increase of 8−12 nm.[12,47]

Apo AI-SH addition to the phospholipids does not result in a significant increase in diameter. This is consistent with the snorkel model of Apo AI interaction with phospholipids, which proposes that Apo AI nestles in the phospholipids such that the nonpolar face of the Apo AI α-helices interacts with the phospholipid tails while the polar face interacts with the charged head groups and solvent.[48] Thus, the nestling of Apo AI in the phospholipid layer would not be expected to lead to a large increase in size. In addition, there is only a small difference, 1−4 nm, in diameter between HDL Au NPs with the same surface composition but synthesized using a different size of Au NP template. Thus, the measured 2 nm difference in template core size correlates well with the small difference in HDL Au NP conjugate size when using different templates.

Drying effects and uranyl acetate staining may affect the diameter of the HDL Au NPs measured by TEM. Thus, dynamic light scattering (DLS) was also used to measure the hydrodynamic diameter of the HDL biomimics (Figure 3). The DLS measurements correlate with the TEM data. They show the difference in thickness between the monolayer and bilayer lipid functionalizations and little change in size after the addition

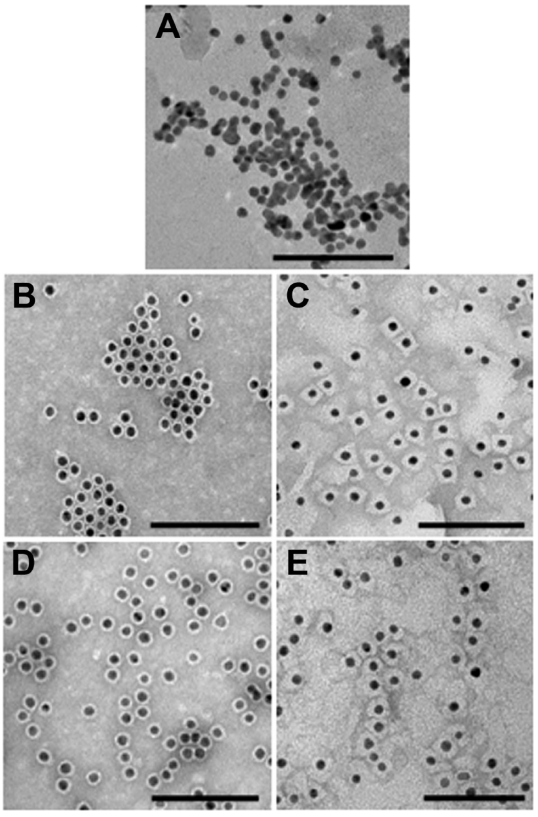

Figure 2. Transmission electron microscopy images of HDL Au NPs stained with uranyl acetate: (A) 8 nm Au NP colloid, (B) 8 nm monolayer, (C) 8 nm bilayer, (D) 8 nm Apo monolayer, (E) 8 nm Apo bilayer. All scale bars are 100 nm.

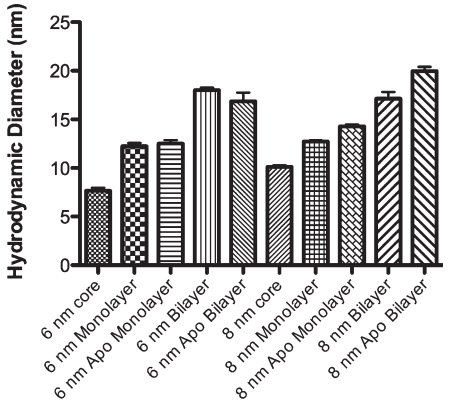

Figure 3. Hydrodynamic diameters of HDL Au NPs measured by DLS.

of Apo AI-SH. Overall, the sizes of the HDL Au NPs are comparable to those of mature spherical HDLs.[43]

Fluorophore-labeled Apo AI-SH was used to quantify the number of proteins per HDL Au NP. The HDL Au NPs were synthesized with fluorophore-labeled Apo AI-SH. After synthesis, the Au NP template was dissolved to remove any fluorescence quenching by the Au NP, and the concentration of Apo AI-SH on the Au NP was determined using a standard curve of fluorophore-labeled Apo AI-SH. HDL Au NPs with a 6 nm core have 2 ± 1 Apo AI-SH, while the 8 nm core HDL Au NPs contain 7 ± 4 Apo AI-SH for the monolayer and 4 ± 2 for the bilayer surface modifications. The increase in number of Apo AI-SH on the larger core is reasonable given the increase in surface area. Furthermore, the number of proteins on the HDL Au NPs of both core sizes is in agreement with the number of Apo AI on HDLs purified from human serum as they have been shown to contain 3–7 Apo AI molecules.[17] After characterizing some of the key physical properties of the HDL Au NPs, we investigated their cholesterol sequestration properties.

TABLE 1. Dissociation Constants (K_d) for HDL Au NPs Binding Cholesterol

K_d (nM)	core size	monolayer	bilayer
without Apo AI	6 nm	0.3 ± 0.5	60 ± 20
with Apo AI		0.5 ± 0.7	70 ± 10
without Apo AI	8 nm	80 ± 40	830 ± 90
with Apo AI		150 ± 60	650 ± 60

Analysis of Cholesterol Binding in Solution by the HDL Au NPs. The ability of the HDL Au NPs to bind cholesterol in solution was analyzed using cholesterol with a fluorophore label. NBD cholesterol is minimally fluorescent in polar environments but becomes fluorescent in nonpolar surroundings such as a phospholipid layer.[49] This cholesterol analogue has been studied extensively and reportedly mimics the behavior of natural cholesterol.[49] For all of the HDL Au NPs, NBD cholesterol binding parameters were determined by incubating the constructs with increasing concentrations of NBD cholesterol, measuring the fluorescence, and generating binding isotherms.

Two binding parameters were used to evaluate cholesterol binding. The dissociation constant (K_d) is the concentration at which half of the ligand is bound at equilibrium.[50] This value is larger for HDL biomimics synthesized using an 8 nm core when comparing constructs with the same surface chemistry (Table 1). The measured K_d is approximately an order of magnitude larger for the bilayer than for the monolayer surface functionalization for HDL Au NPs with the same core size. There is no significant difference in K_d when Apo AI-SH is present or absent from the HDL Au NPs.

The maximum specific binding (B_{max}) provides information on the capacity of the construct to bind cholesterol.[51] The same trends were observed for B_{max} as found for K_d. When comparing constructs with the same surface modification, B_{max} is larger for constructs with an 8 nm core than a 6 nm core (Table 2). For HDL Au NPs with the same core size, B_{max} is more than 10-fold greater for the bilayer than for the monolayer surface chemistry. The presence or absence of Apo AI-SH does not appreciably change B_{max} values as they are similar for HDL Au NPs with and without Apo AI-SH

TABLE 2. Cholesterol Maximum Specific Binding (B_{max}) for HDL Au NPs

B_{max} (10^3 cps)[a]	core size	monolayer	bilayer
without Apo AI	6 nm	3.6 ± 0.4	50 ± 10
with Apo AI		5.1 ± 0.7	62 ± 5
without Apo AI	8 nm	10 ± 1	420 ± 20
with Apo AI		12 ± 2	330 ± 10

[a] Unit cps is counts per second, the relative fluorescence intensity of the bound cholesterols and not number of molecules bound.

and having the same core size and phospholipid modification.

Determination of Cholesterol Efflux by the HDL Au NPs. Having quantified the ability of each of the HDL Au NPs to bind cholesterol in solution, we sought to establish how these binding parameters translate into relevant cell culture models of free cholesterol efflux. Additionally, we compared the synthetic HDL biomimics to known cholesterol acceptors, namely, Apo AI and human serum derived HDL. Human and murine macrophage cells enriched with free cholesterol and radiolabeled cholesterol (^{3}H-cholesterol) were used to compare the ability of the HDL biomimics to efflux cholesterol. HDL Au NPs were incubated with the cells for 48 h in the presence of an LXR agonist, which increases the expression of cholesterol efflux receptors on the cell surface.[52,53] Treating the cells with an LXR agonist generated more robust cholesterol efflux (see Supporting Information Figures S4 and S5 for efflux without LXR agonist treatment). The concentrations of purified Apo AI, natural HDL and 6 nm core HDL Au NPs were normalized to contain the same concentration of Apo AI. When testing the cholesterol efflux dose response to 8 nm core HDL Au NPs, we found that maximum cholesterol efflux occurred at an HDL Au NP concentration that was lower than for constructs synthesized with a 6 nm core (Supporting Information Figure S6). Thus, to ensure the maximum amount of cholesterol efflux to all acceptors, a lower concentration of 8 nm core HDL Au NPs was used. The concentration of HDL Au NPs without Apo AI-SH was normalized to the same Au NP concentration as the HDL Au NPs with Apo AI-SH.

In general, HDL Au NPs with a phospholipid monolayer display little to no ability to efflux cholesterol from macrophage cells, while HDL Au NPs functionalized with a phospholipid bilayer having the same core size and Apo AI-SH content cause significantly more cholesterol efflux ($P < 0.05$, Figure 4). Cells treated with HDL Au NPs without Apo AI-SH also exhibit very little cholesterol efflux. Inclusion of Apo AI-SH in the surface functionalization results in enhanced cholesterol efflux, ranging from 2- to 40-fold depending on the core size and phospholipid covering. The addition of Apo AI-SH has a much greater effect when a phospholipid monolayer is used compared to a bilayer. Furthermore,

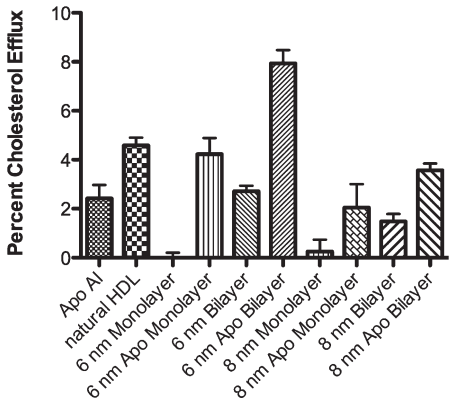

Figure 4. Cholesterol efflux from human (THP-1) macrophage cells. Human macrophage cells were loaded with free cholesterol and ^{3}H-cholesterol, equilibrated with medium containing 3 μM LXR agonist, and then treated with the cholesterol acceptors for 48 h. Concentrations of cholesterol acceptors: 150 nM Apo AI, 50 nM natural HDL, 50 nM for all 6 nm core HDL Au NPs, and 5 nM for all 8 nm core HDL Au NPs.

constructs with an 8 nm core elicit less cholesterol efflux than constructs with a 6 nm core and the same surface modification. Since increasing the concentration of the 8 nm core HDL Au NPs was found to decrease cholesterol efflux, the effect of different core sizes on cholesterol efflux is due to the HDL Au NP and not the difference in treatment concentration. Similar trends were observed with murine (J774) macrophage cells (Supporting Information Figure S7).

With respect to purified natural HDL and Apo AI, many of the HDL biomimics cause cholesterol efflux on the same order of magnitude as one of these two natural molecules. Three of the HDL Au NPs generate cholesterol efflux similar to Apo AI: 6 nm core with a bilayer, 8 nm core with Apo AI-SH and a monolayer, and 8 nm core with a bilayer. The 6 nm core with Apo AI-SH and a monolayer and the 8 nm core with Apo AI-SH and a bilayer efflux similar percentages of cholesterol as natural HDL. The 6 nm core with Apo AI-SH and a bilayer effluxes significantly more cholesterol than any of the other treatments including natural HDL at the concentrations used ($P < 0.05$). Similar results of cholesterol efflux were obtained for murine macrophage cells (Supporting Information Figure S7).

In order to determine if the 6 nm core HDL Au NPs with Apo AI-SH and a phospholipid bilayer efflux cholesterol *via* mechanisms utilized by natural HDL, we conducted a competition experiment. Macrophages were treated with HDL Au NPs and increasing concentrations of human HDL. The data show that, as the concentration of human HDL included in the media increased, the amount of ^{3}H-cholesterol effluxed to and bound by the HDL Au NPs decreased (Supporting Information Figure S8). The decrease in the cholesterol bound by the HDL Au NPs indicates that natural HDL competes with the HDL Au NP as an acceptor of

cholesterol and suggests that HDL Au NPs employ similar pathways as natural HDL to efflux cholesterol from macrophages.

DISCUSSION

In this work, we utilized a gold nanoparticle template to synthesize HDL biomimics and investigated the effect of template size and surface chemistry on cholesterol binding and efflux in cell culture models. Characterization of the HDL Au NPs indicates that all of the constructs mimic the general physical and structural properties of natural HDL.[3,17,43] TEM analysis of the Au NPs showed that the sizes were 6 ± 1 and 8 ± 1 nm in diameter. This subtle difference in template size has a small but measurable impact on the final size of the constructs and a clear effect on the functional properties of the HDL Au NPs.

The binding parameters K_d and B_{max} were utilized to characterize the ability of the HDL Au NPs to sequester cholesterol in solution. HDL Au NPs with a monolayer of phospholipids have a lower K_d and a lower B_{max} than constructs with a bilayer, indicating that they bind cholesterol more tightly than bilayer biomimics but to a lesser overall extent (Tables 1 and 2). We hypothesize that the lower K_d and B_{max} values are a result of the reduced phospholipid layer thickness and also the method of attachment of the phospholipids. In the case of the monolayer, both fatty acid tails of the phospholipid are attached to the Au NP surface, which limits the thickness and mobility of the phospholipid monolayer. This results in less total cholesterol bound but a tighter complex, which are reflected by the lower K_d and B_{max} values. Indeed, the data suggest minimal cholesterol is bound by the monolayer constructs. In contrast, only the inner phospholipid layer is attached to the Au NP for the HDL biomimics functionalized with a bilayer, and the attachment is *via* the phospholipid head group. This generates a thicker phospholipid layer with greater mobility and may contribute to the observed increase in K_d for the bilayer constructs. Furthermore, the increased thickness of the phospholipid bilayer sequesters more cholesterol as demonstrated by a larger B_{max}.

In general, the addition of Apo AI-SH to the HDL Au NP does not greatly change the measured K_d and B_{max} for cholesterol in solution. For most of the constructs, there is a small increase in the values when Apo AI-SH is present. Apo AI is a protein consisting of repeating amphipathic α-helices.[54] In general, one face of each α-helix is nonpolar, while the other is polar.[48,54] Studies show that the nonpolar faces of the α-helices interact with the phospholipid tails while the polar portions interact with the phospholipid head groups and are exposed to solvent.[48] The small increase in K_d may be accounted for by the interaction of Apo AI with the phospholipids on the Au NP. This interaction may decrease the hydrophobic interactions between the phospholipids that lead to cholesterol binding and therefore decrease the binding strength. Moreover, the protein may create additional sites in which cholesterol can be sequestered, thus increasing the cholesterol carrying capacity as indicated by a larger B_{max}. However, as the binding parameters are very similar with and without Apo AI-SH, any changes to the phospholipid layer by Apo AI have minimal effect on the ability of the HDL Au NPs to bind cholesterol in solution.

The results show that the core size of biomimetic HDL Au NPs is an important factor for cholesterol binding. Increasing the size of the Au NP core from 6 to 8 nm led to an increase in the K_d and B_{max}, indicating a significant decrease in cholesterol binding strength but a significant increase in binding capacity. This behavior was observed for each of the surface chemistries explored, both monolayer and bilayer, and with and without Apo AI. Since the overall size of the constructs does not significantly change by increasing the template core size, the difference in cholesterol binding and capacity is not simply due to a difference in surface area. The difference in radius of curvature of the core likely affects the adsorption and packing of phospholipids on the Au NP surface and thus may affect the ability of the constructs to bind cholesterol.

The cell culture experiments clearly demonstrate the contribution of phospholipid surface chemistry and the importance of Apo AI on the ability of HDL Au NPs to mimic natural HDL. Despite the lack of Apo AI, the 6 nm core HDL Au NP with a bilayer demonstrates cholesterol efflux equal to that of purified Apo AI while the same core with a monolayer exhibits no cholesterol efflux. This result shows that the efflux is a result of the difference in phospholipid surface chemistry and not just the presence or absence of Apo AI. Furthermore, inclusion of Apo AI-SH on the HDL Au NP increases the amount of cholesterol efflux by at least 2-fold for the bilayer HDL Au NPs and more than 10-fold for the monolayer surface compositions. This is expected, as Apo AI is known to be important for interacting with cell surface proteins responsible for cholesterol efflux, such as the ATP-binding cassette transporters A1 (ABCA1) and G1 (ABCG1) and the scavenger receptor class B type I (SR-BI).[55] Significantly, an LXR agonist was used to increase the expression of ABCA1 and ABCG1,[52,53] which resulted in greater efflux to cholesterol acceptors, particularly HDL Au NPs with Apo AI-SH. The increase in efflux indicates that HDL Au NPs with Apo AI-SH are able to access cholesterol through active efflux pathways.[56] In particular, the 6 nm core HDL Au NP with Apo AI-SH and a phospholipid bilayer exhibits nearly 2-fold greater cholesterol efflux than the purified human HDL used as a positive control. Moreover, human HDL competes with the 6 nm core HDL Au NP with Apo AI-SH and a bilayer for cholesterol, suggesting that both particles efflux cholesterol through

similar pathways. We therefore conclude that an Apo AI-SH and phospholipid bilayer surface chemistry best mimics the structure and function of naturally occurring HDL and is the optimal architecture evaluated in these studies. Furthermore, with respect to the sizes of Au NP templates tested, a 6 nm Au NP generates a more functional biomimic than an 8 nm Au NP.

These data illustrate the promise of inorganic nanoparticles for synthesizing biologically active HDL mimics with tailorable functionality. By changing the size of the Au NP and the surface chemistry, we have established the ability to synthesize HDL biomimics with different cholesterol binding properties. Furthermore, we have demonstrated the importance of core size, phospholipid surface chemistry, and presence of Apo AI in synthesizing structures that mimic naturally occurring HDL by effluxing cholesterol from macrophage cells. As the size, shape, and surface chemistry of natural HDLs are currently under intense investigation with regard to function, this work demonstrates that a templated approach to spherical HDL synthesis may provide a unique opportunity to further probe structure–function relationships and the biological activity of spherical HDL. In addition, this study highlights the potential of using nanoparticle templates for synthesizing functional HDL biomimics for therapeutic purposes.

METHODS

Synthesis of 1,2-Bis(16-mercaptohexadecanoyl)-*sn*-glycero-3-phosphocholine. 1,2-Bis(16-mercaptohexadecanoyl)-*sn*-glycero-3-phosphocholine (L16SH) was synthesized following the synthesis reported by Coyle *et al.*[57] Full characterization is available in the Supporting Information.

Synthesis of the HDL Au NPs. Citrate-stabilized colloidal gold nanoparticles (Au NPs), 5 and 10 nm in diameter, were purchased from Ted Pella. TEM analysis, however, showed that they are 6 ± 1 and 8 ± 1 nm in diameter. Phospholipids, with the exception of the sulfhydryl-modified phospholipid, were obtained from Avanti Polar Lipids. Apolipoprotein AI (Apo AI) was purchased from Meridian Life Science, Inc. Zeba columns and 2-iminothiolane (Traut's reagent) were purchased from Thermo Fisher Scientific. Ethylenediaminetetraacetic acid (EDTA) at pH 8.0 came from Ambion. Ethanol was obtained from Sigma-Aldrich. Ultrapure (18.2 MΩ) water was used during synthesis of the HDL Au NPs and for all experiments. All items, except Apo AI, were used as purchased.

Sulfhydryl groups were added to Apo AI using Traut's reagent to modify the protein for nanoparticle attachment. Traut's reagent reacts with the primary amines that reside on lysine residues to generate amino acids with sulfhydryl groups.[58] Apo AI was reconstituted in a small amount of PBS containing 4 mM EDTA at pH 8.0. A 20-fold molar excess of Traut's reagent was added and allowed to incubate with the protein for 1 h at room temperature (RT). The modified Apo AI (Apo AI-SH) was then purified with a Zeba column.

For the HDL Au NPs containing Apo AI-SH, the protein was added to the Au colloid in a 5-fold (6 nm Au NPs) or 10-fold (8 nm Au NPs) molar excess. After incubation with Apo AI-SH (10 h, RT), phospholipids were added. The phospholipids were dissolved in ethanol, and fresh solutions of 1 mM were used for each synthesis.

In constructing monolayer HDL Au NPs, the Au NPs containing Apo AI-SH were diluted 50% with ethanol. The sulfhydryl-modified phospholipid, L16SH, was added in 1000-fold (6 nm Au NPs) or 5000-fold (8 nm Au NPs) molar excess. The solutions were incubated (10 h, RT) and subsequently purified by diafiltration using a KrosFlo Research II tangential flow filtration system (Spectrum Laboratories) fitted with a 50 kDa modified polyethersulfone (mPES) module. For all purifications, the buffer was exchanged at least seven times to remove unreacted Apo AI-SH and phospholipids. An aqueous solution of 50% ethanol was used at the beginning of the purification and changed to 25% ethanol and, ultimately, to water to aid in phospholipid removal.

Bilayer HDL Au NPs were synthesized following a similar procedure. Before addition of the lipids, the Au NPs functionalized with Apo AI-SH were diluted by 20% with ethanol. Two phospholipids, 1,2-dipalmitoyl-*sn*-glycero-3-phosphoethanolamine-*N*-[3-(2-phyridyldithio)propionate] (PDP PE) and 1,2-dipalmitoyl-*sn*-glycero-3-phosphocholine (DPPC), were both added in 1000-fold (6 nm Au NPs) or 5000-fold (8 nm Au NPs) molar excess. After incubation (10 h, RT), the solutions were purified by diafiltration as above, with the exception that water was used for the entire purification process.

The monolayer and bilayer HDL Au NPs without Apo AI-SH were synthesized in a manner similar to that described for the HDL Au NPs with the protein. Au colloid was diluted by either 50 or 20% with ethanol for the monolayer or bilayer modification, respectively. Phospholipids were added in 1000-fold (6 nm Au NPs) or 5000-fold (8 nm Au NPs) molar excess. The solutions were incubated (10 h, RT) and purified by diafiltration. A 30 kDa mPES module was used for the purification. The monolayer HDL Au NPs were initially purified with 50% ethanol, then 25% ethanol, and then water. Water was used for the entire purification of the bilayer HDL Au NPs.

Characterization of the HDL Au NPs. All absorbance measurements were taken on a Varian Cary 5000 UV–vis–NIR spectrophotometer (Agilent Technologies). DLS measurements were performed on a Zetasizer Nano ZS (Malvern Instruments Ltd.).

The uranyl acetate (UA) used for transmission electron microscopy (TEM) was purchased from Ted Pella, Inc. Copper grids (200 mesh) with a carbon film were obtained from Electron Microscopy Sciences. For negative staining, the Au colloid or HDL Au NPs were first deposited on the grid and then stained by floating the grid face down in a drop of 2% UA. The grids were dried on filter paper prior to imaging with a Tecnai Spirit G2 (FEI) TEM.

Alexa Fluor 488 was obtained from Invitrogen for fluorophore labeling of Apo AI. Phosphate buffered saline (PBS) came from Thermo Fisher Scientific. Potassium cyanide (KCN) and Tween were purchased from Sigma-Aldrich. Fluorescence measurements were made on a FluoDia T70 fluorescence microplate reader (Photon Technology International). Apo AI was labeled with Alexa Fluor 488 per kit instructions. Briefly, 50 μL of 1 M sodium bicarbonate and 50 μL of PBS were added to 450 μL 1 mg/mL Apo AI, and the solution was added to the vial containing Alexa Fluor 488. The protein was incubated with the dye (1 h, RT). Unconjugated dye was removed by running the protein on the column and purification resin provided by Invitrogen. After collecting the protein fraction, the concentration of Apo AI and of Alexa Fluor 488 was determined from the absorbance of the labeled Apo AI at 280 and 494 nm corresponding to the protein and the dye, respectively. The protein was then modified with Traut's reagent as described previously. HDL Au NPs were synthesized with fluorophore-modified Apo AI-SH. After purification as described previously, aliquots of the HDL Au NPs containing the same concentration of Au NPs were dissolved in PBS containing 0.01% Tween and 80 mM KCN. The fluorescence of the dissolved HDL Au NPs was measured and the concentration of Apo AI calculated from a standard curve of fluorophore-labeled Apo AI-SH.

Analysis of Cholesterol Binding. Cholesterol binding measurements were taken on a Fluorolog spectrafluorometer (HORIBA).

The data were analyzed using GraphPad Prism (GraphPad Software) and the one-site specific binding analysis. 25-[*N*-[(7-Nitro-2-1,3-benzoxadiazol-4-yl)methyl]amino]-27-norcholesterol (NBD cholesterol) was purchased from Avanti Polar Lipids, and dimethyl formamide (DMF) came from Sigma-Aldrich. Solutions of NBD cholesterol ranging from 0 to 750 nM were made in DMF. HDL Au NPs were incubated (1 h, RT) with 5 μL of the different concentrations of NBD cholesterol, and the fluorescence was measured for each concentration. The fluorescence values were plotted as a function of NBD cholesterol concentration and the plots analyzed in Graphpad Prism to determine the dissociation constant (K_d) and maximum specific binding (B_{max}) values for each HDL Au NP.

Cell Culture and Assay of Cellular Cholesterol Efflux. Both human and murine cell culture models were used to measure cholesterol efflux to HDL Au NPs. The human monocytic leukemia cell line THP-1 and mouse macrophage cell line J774 were purchased from American Type Culture Collection (ATCC). [1, 2-^{3}H(*N*)]-Cholesterol (^{3}H-cholesterol) was obtained from Perkin-Elmer. Bovine serum albumin (BSA), phorbol 12-myristate 13-acetate (PMA), and free cholesterol were obtained from Sigma-Aldrich. Human HDL was purchased from EMD Chemicals (Merck KGaA, Darmstadt, Germany), and purified Apo AI was purchased from Meridian Life Science, Inc. The LXR agonist *N*-(2, 2, 2-trifluoroethyl)-*N*-[4-[2, 2, 2-trifluoro-1-hydroxy-1-(trifluoromethyl)ethyl]phenyl]benzene-sulfonamide was obtained from Cayman Chemical Company (Ann Arbor, MI).

THP-1 and J774 cells were cultured in RPMI-1640 and DMEM, respectively. All of the culture media were supplemented with 10% FBS and penicillin/streptomycin (100 units/mL and 100 μg/mL, respectively). The cells were cultured at 37 °C in a humidified 5% CO_2 atmosphere.

THP-1 cells were added to 24-well plates at 1.5×10^5/well and cultured for 72 h in the presence of 100 nM PMA to induce cell differentiation. J774 cells were seeded to 24-well plates at 8×10^4/well and cultured for 24 h. Cells were then washed with PBS and loaded/labeled with fresh media plus 1% BSA, 5 μM free cholesterol, and 1 μCi/mL ^{3}H-cholesterol for 24 h and subsequently incubated overnight in media containing 0.2% BSA with or without 3 μM of LXR agonist. After removing the media, the cells were washed twice with PBS and exposed to different cholesterol acceptors in fresh culture media for 48 h. At the end of the efflux period, the efflux media were collected and centrifuged at 4 °C for 5 min at 2000 rpm to remove floating cells. The supernatant was collected and subjected to liquid scintillation counting. The cell monolayer was washed with PBS, and the cellular lipids were extracted with isopropyl alcohol and measured by liquid scintillation counting. The percentage of cholesterol efflux was determined for each well using the formula: $\text{counts}_{\text{media}}/(\text{counts}_{\text{cells}} + \text{counts}_{\text{media}}) \times 100$. The background cholesterol efflux obtained in the absence of any acceptor was subtracted from the efflux values obtained with the cholesterol acceptors.

For the competition experiment, differentiated THP-1 cells were loaded and labeled with cholesterol and equilibrated as previously described. The cells were washed with PBS and then incubated for 16 h with 50 nM HDL Au NPs (6 nm core, Apo AI-SH, and phospholipid bilayer) and increasing concentrations of human HDL. After the incubation, the culture media (500 μL in each well) were collected and centrifuged at 500*g* for 10 min to pellet the dead cells. Then 400 μL of supernatant was transferred to new Eppendorf tubes and centrifuged at 15 000 rpm for 30 min to pellet the HDL Au NPs. After centrifugation, 300 μL of supernatant was transferred to scintillation vials for liquid scintillation counting. The HDL Au NPs in the remaining 100 μL of media were resuspended in 200 μL of PBS and transferred to scintillation vials for liquid scintillation counting. The cell monolayer was treated as previously described and analyzed by liquid scintillation counting. The percentage of cholesterol efflux to the HDL Au NPs was determined for each well using the formula: $\text{counts}_{\text{HDL Au NP pellet}}/(\text{counts}_{\text{cells}} + \text{counts}_{\text{media}} + \text{counts}_{\text{HDL Au NP pellet}}) \times 100$.

Statistical Analysis. Statistical analyses were completed using GraphPad Prism (GraphPad Software). Cholesterol efflux to HDL Au NPs having different phospholipid layers with the same core size and Apo AI composition were compared using an unpaired *t* test. The amount of cholesterol efflux to the 6 nm core Apo AI-SH bilayer construct was compared to all other treatments by a one-way analysis of variance (ANOVA) and Dunnett's multiple comparison test. A p value <0.05 was considered significant.

Acknowledgment. C.S.T. would like to thank Howard Hughes Medical Institute for an Early Career Physician-Scientist award. A.J.L. thanks the Northwestern University Ryan Fellowship for support. C.A.M. acknowledges support from the NCI-CCNE at Northwestern University, an NSF NSEC grant, and an Air Force Office of Scientific Research grant. Imaging work was performed at the Northwestern University Cell Imaging Facility generously supported by NCI CCSG P30 CA060553 awarded to the Robert H. Lurie Comprehensive Cancer Center.

Supporting Information Available: Characterization of 1,2-bis(16-mercaptohexadecanoyl)-*sn*-glycero-3-phosphocholine (L16SH), UV−vis spectra of all the HDL Au NPs, TEM images of the 6 nm core HDL Au NPs, cholesterol efflux from macrophage cells without LXR agonist treatment, the effect of 8 nm core HDL Au NP concentration on cholesterol efflux, cholesterol efflux from murine macrophage cells with LXR agonist treatment, and cholesterol efflux in the presence of increasing concentrations of human HDL. This material is available free of charge *via* the Internet at http://pubs.acs.org.

REFERENCES AND NOTES

1. Mackay, J.; Mensah, G. A. *Atlas of Heart Disease and Stroke*; World Health Organization and Centers for Disease Control and Prevention, 2004.
2. Falk, E. Pathogenesis of Atherosclerosis. *J. Am. Coll. Cardiol.* **2006**, *47*, C7–C12.
3. Genest, J.; Libby, P. Lipoprotein Disorders and Cardiovascular Disease. In *Braunwald's Heart Disease: A Textbook of Cardiovascular Medicine [Online]*, 9th ed.; Bonow, R. O., Mann, D. L., Zipes, D. P., Libby, P., Eds; Elsevier Saunders: Philadelphia, PA, 2011; pp 975−994; http://www.mdconsult.com.ezproxy.galter.northwestern.edu/books/page.do?eid=4-u1.0-B978-1-4377-0398-6.00047-0&isbn=978-1-4377-0398-6&uniqId=303440482-2#4-u1.0-B978-1-4377-0398-6.00047-0 (accessed August 8, 2011).
4. Glass, C. K.; Witztum, J. L. Atherosclerosis: The Road Ahead. *Cell* **2001**, *104*, 503–516.
5. Lusis, A. J. Atherosclerosis. *Nature* **2000**, *407*, 233–241.
6. Singh, I. M.; Shishehbor, M. H.; Ansell, B. J. High-Density Lipoprotein as a Therapeutic Target: A Systematic Review. *JAMA, J. Am. Med. Assoc.* **2007**, *298*, 786–798.
7. Gordon, T.; Castelli, W. P.; Hjortland, M. C.; Kannel, W. B.; Dawber, T. R. High-Density Lipoprotein as a Protective Factor against Coronary Heart-Disease—Framingham Study. *Am. J. Med.* **1977**, *62*, 707–714.
8. Calabresi, L.; Gomaraschi, M.; Rossoni, G.; Franceschini, G. Synthetic High Density Lipoproteins for the Treatment of Myocardial Ischemia/Reperfusion Injury. *Pharmacol. Ther.* **2006**, *111*, 836–854.
9. Ikonen, E. Cellular Cholesterol Trafficking and Compartmentalization. *Nat. Rev. Mol. Cell Biol.* **2008**, *9*, 125–138.
10. Nissen, S. E.; Tsunoda, T.; Tuzcu, E. M.; Schoenhagen, P.; Cooper, C. J.; Yasin, M.; Eaton, G. M.; Lauer, M. A.; Sheldon, W. S.; Grines, C. L.; *et al.* Effect of Recombinant ApoA-I Milano on Coronary Atherosclerosis in Patients with Acute Coronary Syndromes: A Randomized Controlled Trial. *JAMA, J. Am. Med. Assoc.* **2003**, *290*, 2292–2300.
11. Nicholls, S. J.; Uno, K.; Kataoka, Y.; Nissen, S. E. ETC-216 for Coronary Artery Disease. *Expert Opin. Biol. Ther.* **2011**, *11*, 387–394.
12. Jonas, A. Reconstitution of High-Density-Lipoproteins. *Methods Enzymol.* **1986**, *128*, 553–582.
13. Silva, R. A. G. D.; Huang, R.; Morris, J.; Fang, J.; Gracheva, E. O.; Ren, G.; Kontush, A.; Jerome, W. G.; Rye, K. A.; Davidson, W. S. Structure of Apolipoprotein A-I in Spherical High Density Lipoproteins of Different Sizes. *Proc. Natl. Acad. Sci. U.S.A.* **2008**, *105*, 12176–12181.

14. Wang, M. H.; Briggs, M. R. HDL: The Metabolism, Function, and Therapeutic Importance. *Chem. Rev.* **2004**, *104*, 119–137.
15. Davidson, W. S.; Thompson, T. B. The Structure of Apolipoprotein A-I in High Density Lipoproteins. *J. Biol. Chem.* **2007**, *282*, 22249–22253.
16. Thomas, M. J.; Bhat, S.; Sorci-Thomas, M. G. Three-Dimensional Models of HDL ApoA-I: Implications for Its Assembly and Function. *J. Lipid Res.* **2008**, *49*, 1875–1883.
17. Huang, R.; Silva, R. A. G. D.; Jerome, W. G.; Kontush, A.; Chapman, M. J.; Curtiss, L. K.; Hodges, T. J.; Davidson, W. S. Apolipoprotein A-1 Structural Organization in High-Density Lipoproteins Isolated from Human Plasma. *Nat. Struct. Mol. Biol.* **2011**, *18*, 416–423.
18. Asztalos, B. F.; Tani, M.; Schaefer, E. J. Metabolic and Functional Relevance of HDL Subspecies. *Curr. Opin. Lipidol.* **2011**, *22*, 176–185.
19. Asztalos, B. F.; Cupples, L. A.; Demissie, S.; Horvath, K. V.; Cox, C. E.; Batista, M. C.; Schaefer, E. J. High-Density Lipoprotein Subpopulation Profile and Coronary Heart Disease Prevalence in Male Participants of the Framingham Offspring Study. *Arterioscler., Thromb., Vasc. Biol.* **2004**, *24*, 2181–2187.
20. Asztalos, B. F.; Collins, D.; Cupples, L. A.; Demissie, S.; Horvath, K. V.; Bloomfield, H. E.; Robins, S. J.; Schaefer, E. J. Value of High-Density Lipoprotein (HDL) Subpopulations in Predicting Recurrent Cardiovascular Events in the Veterans Affairs HDL Intervention Trial. *Arterioscler., Thromb., Vasc. Biol.* **2005**, *25*, 2185–2191.
21. Movva, R.; Rader, D. J. Laboratory Assessment of HDL Heterogeneity and Function. *Clin. Chem.* **2008**, *54*, 788–800.
22. Daniel, M. C.; Astruc, D. Gold Nanoparticles: Assembly, Supramolecular Chemistry, Quantum-Size-Related Properties, and Applications toward Biology, Catalysis, and Nanotechnology. *Chem. Rev.* **2004**, *104*, 293–346.
23. Mirkin, C. A.; Letsinger, R. L.; Mucic, R. C.; Storhoff, J. J. A DNA-Based Method for Rationally Assembling Nanoparticles into Macroscopic Materials. *Nature* **1996**, *382*, 607–609.
24. Elghanian, R.; Storhoff, J. J.; Mucic, R. C.; Letsinger, R. L.; Mirkin, C. A. Selective Colorimetric Detection of Polynucleotides Based on the Distance-Dependent Optical Properties of Gold Nanoparticles. *Science* **1997**, *277*, 1078–1081.
25. Rosi, N. L.; Giljohann, D. A.; Thaxton, C. S.; Lytton-Jean, A. K. R.; Han, M. S.; Mirkin, C. A. Oligonucleotide-Modified Gold Nanoparticles for Intracellular Gene Regulation. *Science* **2006**, *312*, 1027–1030.
26. Lee, J. S.; Lytton-Jean, A. K. R.; Hurst, S. J.; Mirkin, C. A. Silver Nanoparticle−Oligonucleotide Conjugates Based on DNA with Triple Cyclic Disulfide Moieties. *Nano Lett.* **2007**, *7*, 2112–2115.
27. Giljohann, D. A.; Seferos, D. S.; Daniel, W. L.; Massich, M. D.; Patel, P. C.; Mirkin, C. A. Gold Nanoparticles for Biology and Medicine. *Angew. Chem., Int. Ed.* **2010**, *49*, 3280–3294.
28. Cutler, J. I.; Zheng, D.; Xu, X. Y.; Giljohann, D. A.; Mirkin, C. A. Polyvalent Oligonucleotide Iron Oxide Nanoparticle "Click" Conjugates. *Nano Lett.* **2010**, *10*, 1477–1480.
29. Cutler, J. I.; Zhang, K.; Zheng, D.; Auyeung, E.; Prigodich, A. E.; Mirkin, C. A. Polyvalent Nucleic Acid Nanostructures. *J. Am. Chem. Soc.* **2011**, *133*, 9254–9257.
30. Feldherr, C. M.; Lanford, R. E.; Akin, D. Signal-Mediated Nuclear Transport in Simian-Virus 40-Transformed Cells Is Regulated by Large Tumor-Antigen. *Proc. Natl. Acad. Sci. U.S.A.* **1992**, *89*, 11002–11005.
31. El-Sayed, I. H.; Huang, X. H.; El-Sayed, M. A. Surface Plasmon Resonance Scattering and Absorption of Anti-EGFR Antibody Conjugated Gold Nanoparticles in Cancer Diagnostics: Applications in Oral Cancer. *Nano Lett.* **2005**, *5*, 829–834.
32. Kim, Y. P.; Daniel, W. L.; Xia, Z. Y.; Xie, H. X.; Mirkin, C. A.; Rao, J. H. Bioluminescent Nanosensors for Protease Detection Based upon Gold Nanoparticle−Luciferase Conjugates. *Chem. Commun.* **2010**, *46*, 76–78.
33. Xie, H.; Tkachenko, A. G.; Glomm, W. R.; Ryan, J. A.; Brennaman, M. K.; Papanikolas, J. M.; Franzen, S.; Feldheim, D. L. Critical Flocculation Concentrations, Binding Isotherms, and Ligand Exchange Properties of Peptide-Modified Gold Nanoparticles Studied by UV−Visible, Fluorescence, and Time-Correlated Single Photon Counting Spectroscopies. *Anal. Chem.* **2003**, *75*, 5797–5805.
34. Patel, P. C.; Giljohann, D. A.; Seferos, D. S.; Mirkin, C. A. Peptide Antisense Nanoparticles. *Proc. Natl. Acad. Sci. U.S.A.* **2008**, *105*, 17222–17226.
35. Corbierre, M. K.; Cameron, N. S.; Sutton, M.; Mochrie, S. G. J.; Lurio, L. B.; Ruhm, A.; Lennox, R. B. Polymer-Stabilized Gold Nanoparticles and Their Incorporation into Polymer Matrices. *J. Am. Chem. Soc.* **2001**, *123*, 10411–10412.
36. Raula, J.; Shan, J.; Nuopponen, M.; Niskanen, A.; Jiang, H.; Kauppinen, E. I.; Tenhu, H. Synthesis of Gold Nanoparticles Grafted with a Thermoresponsive Polymer by Surface-Induced Reversible-Addition-Fragmentation Chain-Transfer Polymerization. *Langmuir* **2003**, *19*, 3499–3504.
37. Thaxton, C. S.; Daniel, W. L.; Giljohann, D. A.; Thomas, A. D.; Mirkin, C. A. Templated Spherical High Density Lipoprotein Nanoparticles. *J. Am. Chem. Soc.* **2009**, *131*, 1384–1385.
38. Cormode, D. P.; Skajaa, T.; van Schooneveld, M. M.; Koole, R.; Jarzyna, P.; Lobatto, M. E.; Calcagno, C.; Barazza, A.; Gordon, R. E.; Zanzonico, P.; *et al.* Nanocrystal Core High-Density Lipoproteins: A Multimodality Contrast Agent Platform. *Nano Lett.* **2008**, *8*, 3715–3723.
39. Cormode, D. P.; Roessl, E.; Thran, A.; Skajaa, T.; Gordon, R. E.; Schlomka, J. P.; Fuster, V.; Fisher, E. A.; Mulder, W. J. M.; Proksa, R.; *et al.* Atherosclerotic Plaque Composition: Analysis with Multicolor CT and Targeted Gold Nanoparticles. *Radiology* **2010**, *256*, 774–782.
40. Skajaa, T.; Zhao, Y. M.; van den Heuvel, D. J.; Gerritsen, H. C.; Cormode, D. P.; Koole, R.; van Schooneveld, M. M.; Post, J. A.; Fisher, E. A.; Fayad, Z. A.; *et al.* Quantum Dot and Cy5.5 Labeled Nanoparticles To Investigate Lipoprotein Biointeractions *via* Forster Resonance Energy Transfer. *Nano Lett.* **2010**, *10*, 5131–5138.
41. Skajaa, T.; Cormode, D. P.; Jarzyna, P. A.; Delshad, A.; Blachford, C.; Barazza, A.; Fisher, E. A.; Gordon, R. E.; Fayad, Z. A.; Mulder, W. J. M. The Biological Properties of Iron Oxide Core High-Density Lipoprotein in Experimental Atherosclerosis. *Biomaterials* **2011**, *32*, 206–213.
42. McMahon, K. M.; Mutharasan, R. K.; Tripathy, S.; Veliceasa, D.; Bobeica, M.; Shumaker, D. K.; Luthi, A. J.; Helfand, B. T.; Ardehali, H.; Mirkin, C. A.; *et al.* Biomimetic High Density Lipoprotein Nanoparticles for Nucleic Acid Delivery. *Nano Lett.* **2011**, *11*, 1208–1214.
43. Warnick, G. R.; McNamara, J. R.; Boggess, C. N.; Clendenen, F.; Williams, P. T.; Landolt, C. C. Polyacrylamide Gradient Gel Electrophoresis of Lipoprotein Subclasses. *Clin. Lab. Med.* **2006**, *26*, 803–846.
44. Brust, M.; Walker, M.; Bethell, D.; Schiffrin, D. J.; Whyman, R. Synthesis of Thiol-Derivatized Gold Nanoparticles in a 2-Phase Liquid−Liquid System. *J. Chem. Soc., Chem. Commun.* **1994**, 801–802.
45. Mimms, L. T.; Zampighi, G.; Nozaki, Y.; Tanford, C.; Reynolds, J. A. Phospholipid Vesicle Formation and Transmembrane Protein Incorporation Using Octyl Glucoside. *Biochemistry* **1981**, *20*, 833–840.
46. Hatziantoniou, S.; Nezis, I. P.; Margaritis, L. H.; Demetzos, C. Visualisation of Liposomes Prepared from Skin and Stratum Corneum Lipids by Transmission Electron Microscopy. *Micron* **2007**, *38*, 777–781.
47. Jonas, A.; Phillips, M. C. Lipoprotein Structure. In *Biochemistry of Lipids, Lipoproteins and Membranes*, 5th ed.; Vance, D. E., Vance, J. E., Eds.; Elsevier B.V.: Amsterdam, 2008; pp 485−506.
48. Segrest, J. P.; Jones, M. K.; De Loof, H.; Brouillette, C. G.; Venkatachalapathi, Y. V.; Anantharamaiah, G. M. The Amphipathic Helix in the Exchangeable Apolipoproteins: A Review of Secondary Structure and Function. *J. Lipid Res.* **1992**, *33*, 141–166.
49. Chattopadhyay, A. Chemistry and Biology of *N*-(7-Nitrobenz-2-oxa-1,3-diazol-4-yl)-Labeled Lipids—Fluorescent-Probes

of Biological and Model Membranes. *Chem. Phys. Lipids* **1990**, *53*, 1–15.
50. Tetin, S. Y.; Hazlett, T. L. Optical Spectroscopy in Studies of Antibody–Hapten Interactions. *Methods* **2000**, *20*, 341–361.
51. Avdulov, N. A.; Chochina, S. V.; Igbavboa, U.; Warden, C. S.; Schroeder, F.; Wood, W. G. Lipid Binding to Sterol Carrier Protein-2 Is Inhibited by Ethanol. *Biochim. Biophys. Acta, Mol. Cell Biol. Lipids* **1999**, *1437*, 37–45.
52. Waddington, E. I.; Boadu, E.; Francis, G. A. Cholesterol and Phospholipid Efflux from Cultured Cells. *Methods* **2005**, *36*, 196–206.
53. Fiévet, C.; Staels, B. Lixer X Receptor Modulators: Effects on Lipid Metabolism and Potential Use in the Treatment of Atherosclerosis. *Biochem. Pharmacol.* **2009**, *77*, 1316–1327.
54. Frank, P. G.; Marcel, Y. L. Apolipoprotein A-I: Structure–Function Relationships. *J. Lipid Res.* **2000**, *41*, 853–872.
55. Duong, M.; Collins, H. L.; Jin, W. J.; Zanotti, I.; Favari, E.; Rothblat, G. H. Relative Contributions of ABCA1 and SR-BI to Cholesterol Efflux to Serum from Fibroblasts and Macrophages. *Arterioscler., Thromb., Vasc. Biol.* **2006**, *26*, 541–547.
56. Mendez, A. J. Cholesterol Efflux Mediated by Apolipoproteins Is an Active Cellular Process Distinct from Efflux Mediated by Passive Diffusion. *J. Lipid Res.* **1997**, *38*, 1807–1821.
57. Coyle, L. C.; Danilov, Y. N.; Juliano, R. L.; Regen, S. L. Chemisorbed Phospholipid Monolayers on Gold: Well-Defined and Stable Phospholipid Surfaces for Cell Adhesion Studies. *Chem. Mater.* **1989**, *1*, 606–611.
58. Jue, R.; Lambert, J. M.; Pierce, L. R.; Traut, R. R. Addition of Sulfhydryl Groups to *Escherichia coli* Ribosomes by Protein Modification with 2-Iminothiolane (Methyl 4-Mercaptobutyrimidate). *Biochemistry* **1978**, *17*, 5399–5406.